AGU PUBLICATIONS

Space Weather

RESEARCH ARTICLE
10.1002/2016SW001406

Special Section:
Initial Results from the NASA Radiation Dosimetry Experiment (RaD-X) Balloon Flight Mission

Ground-based evaluation of dosimeters for NASA high-altitude balloon flight

T. Straume[1], C. J. Mertens[2], T. C. Lusby[1], B. Gersey[3], W. K. Tobiska[4], R. B. Norman[2], G. P. Gronoff[5], and A. Hands[6]

[1]NASA Ames Research Center, Moffett Field, California, USA, [2]NASA Langley Research Center, Hampton, Virginia, USA, [3]Center for Applied Radiation Research, Prairie View A & M University, Prairie View, Texas, USA, [4]Space Environment Technologies, Pacific Palisades, California, USA, [5]Science Systems and Applications, Inc., Hampton, Virginia, USA, [6]Surrey Space Center, University of Surrey, Guildford, UK

Abstract Results are presented from evaluations of radiation dosimeters prior to a NASA high-altitude balloon flight, the RaD-X mission. Four radiation dosimeters were on board RaD-X: a Far West Hawk (version 3), a Teledyne dosimeter (UDOS001), a Liulin dosimeter (MDU 6SA1), and a RaySure dosimeter (version 3b). The Hawk is a tissue-equivalent proportional counter (TEPC) and the others are solid-state Si sensors. The Hawk served as the "flight standard" and was calibrated for this mission. The Si-based dosimeters were tested to make sure they functioned properly prior to flight but were not calibrated for the radiation environment in the stratosphere. The dosimeters were exposed to ^{60}Co gamma rays and ^{252}Cf fission radiation (which includes both neutrons and gamma rays) at the Lawrence Livermore National Laboratory (LLNL). The measurement results were compared with results from standard "benchmark" measurements of the same sources and source-to-detector distances performed contemporaneously by LLNL calibration facility personnel. For ^{60}Co gamma rays, the dosimeter-to-benchmark ratios were 0.84 ± 0.06, 1.07 ± 0.32, 1.31 ± 0.07, and 0.82 ± 0.24 for the TEPC, Teledyne, Liulin, and RaySure, respectively. For ^{252}Cf radiation, the dosimeter-to-benchmark ratios were 0.94 ± 0.15, 0.55 ± 0.18, 0.58 ± 0.08, and 0.33 ± 0.12 for the TEPC, Teledyne, Liulin, and RaySure. Some examples of how the results were used to help interpret the flight data are also presented.

Key Points:
- Three Si-based dosimeters were functionally tested for the NASA RaD-X mission using ^{60}Co gamma ray and ^{252}Cf fission sources
- Two TEPCs were calibrated, one served as the "flight standard" for comparison and the other as a backup unit
- Ground-based results from all dosimeters and some initial flight results are presented and discussed

Correspondence to:
T. Straume,
Tore.Straume@nasa.gov

Citation:
Straume, T., C. J. Mertens, T. C. Lusby, B. Gersey, W. K. Tobiska, R. B. Norman, G. P. Gronoff, and A. Hands (2016), Ground-based evaluation of dosimeters for NASA high-altitude balloon flight, *Space Weather*, *14*, doi:10.1002/2016SW001406.

Received 22 APR 2016
Accepted 13 SEP 2016
Accepted article online 21 SEP 2016

1. Introduction

Radiation dosimeters selected for a NASA high-altitude balloon flight (the RaD-X mission) were evaluated using standard radiation sources prior to the mission. Here we describe the dosimeters, the radiation sources, and justification for their selection and present the ground-based measurement results. We also present some preliminary results from measurements in the stratosphere that illustrate how the ground-based measurements are used to interpret the flight data. More extensive discussion of flight measurements are provided in companion papers in this special issue [*Mertens et al*., 2016; *Hands et al*., 2016] and are also expected in future publications after further data analysis.

The RaD-X mission was launched 25 September 2015, from Fort Sumner, New Mexico, and was designed in part to provide additional validation of the Nowcast of Atmospheric Ionizing Radiation for Aviation Safety (NAIRAS) model [*Mertens et al*., 2010, 2012, 2013]. A secondary objective was to evaluate compact, low-cost radiation dosimeters for possible future use as continuous monitors on commercial aircraft. A companion paper [*Mertens et al*., 2016] describes the Rad-X mission and the science objectives.

Calculated cosmic ray dose-equivalent (*H*) rates as a function of altitude are illustrated in Figure 1. Primary galactic cosmic ray (GCR) radiations (protons and heavy ions) interact with the upper atmosphere producing a cascade of secondary radiations including neutrons, electrons, muons, and pions. The maximum dose rate is reached at the Pfotzer maximum (the peak in the ionization rate, which occurs at about 20–25 km altitude), where absorbed dose (*D*) rates are about 7–10 μGy/h at mid geomagnetic latitudes during solar minimum [*National Council on Radiation Protection and Measurements (NCRP) Commentary No. 12*, 1995]. With quality factors (*Q*) estimated to be 1.5–3.3 [*O'Brien and Friedberg*, 1994; *Wilson et al*., 1995], this results in *H* rates at the Pfotzer maximum on the order of 10 to 30 μSv/h. This compares with *H* rates at sea level of about 0.03 μSv/h and at commercial airline altitudes (~10 km) of about 5 to 8 μSv/h [*NCRP Commentary No. 12*, 1995].

It is noted that altitude, geomagnetic latitude, and the solar cycle all influence the dose rate. Within the Earth's atmosphere, altitude provides the largest variation in dose rate, except for the rare large solar particle

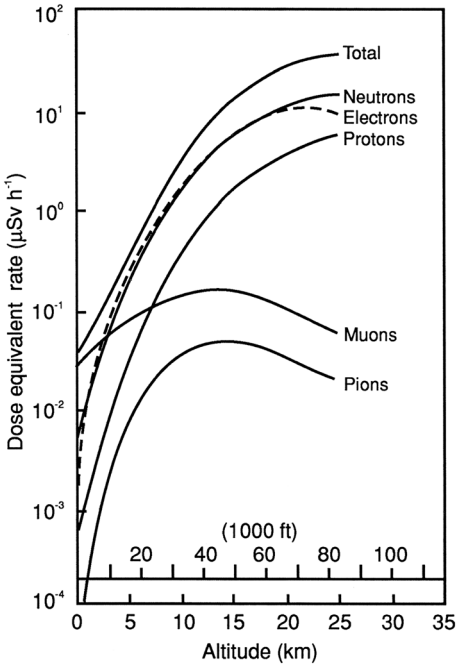

Figure 1. Cosmic radiation dose-equivalent rate as a function of altitude at 55° N geomagnetic latitude during solar minimum [*NCRP*, 1995]. Originally reproduced from *Reitz* [1993] and included here with permission from Oxford University Press.

event, which can pose a hazard to commercial aircraft [e.g., *Langhoff and Straume*, 2012]. Latitude and solar cycle provide a smaller (factor of 2) variation in dose rate.

2. Radiation Dosimeters

Radiation dosimeters selected for the RaD-X mission are (1) a tissue-equivalent proportional counter (TEPC)—the Hawk by Far West Technology, Inc. [*Far West Technologies (FWT)*, 2016; *Conroy*, 2010], (2) a Teledyne total ionizing dose (TID) dosimeter [*Lindstrom et al*., 2011; *Tobiska et al*., 2015], (3) a Liulin linear energy transfer (LET) dosimeter [*Dachev et al*., 2015], and (4) a RaySure dosimeter [*Hands and Dyer*, 2009]. These instruments are described below and were evaluated by exposing them to ground-based National Institute of Standards and Technology (NIST)-traceable gamma ray and neutron radiation sources to ensure that the instruments were functioning correctly prior to flight. Two TEPCs were calibrated using these sources, one was included onboard RaD-X as a "flight standard" for comparison and the other served as a backup unit.

2.1. Far West Tissue-Equivalent Proportional Counter

The TEPC is the de facto instrument for microdosimetry [*International Commission on Radiation Units and Measurements (ICRU)*, 1983] and was selected for the RaD-X mission to serve as a flight standard against which the other dosimeters could be compared. TEPCs have been used for many diverse applications on Earth [e.g., *Straume et al*., 1991; *Lindborg et al*., 1999; *Gersey et al*., 2002; *Lindborg and Nikjoo*, 2011] and in space, including in the Space Shuttle [e.g., *Badhwar et al*., 1996] and in the International Space Station (ISS) [e.g., *Perez-Nunez and Braby*, 2011], and compact TEPC designs are being developed for deep-space human missions [*Straume et al*., 2015].

It is noted that the TEPC can be calibrated for measurements in the stratosphere using commonly available neutron and gamma ray sources. This approach is routinely used to calibrate TEPCs for space, including those placed inside the ISS, where dose rate measurements obtained with the TEPC have been extensively verified by comparing with independent dosimetry and computational modeling methods [e.g., *National Council on Radiation Protection and Measurements Report 132*, 2000; *National Council on Radiation Protection and Measurements Report 153*, 2006]. The standard method is to measure the entire lineal energy (y) spectrum (y is the energy imparted in the TEPC sensitive volume by a single energy deposition event divided by the mean chord length of the spherical detector volume), verify the gas gain using a neutron source to obtain the "proton drop point" (see Figure A2), and employ a gamma ray source to extrapolate the y spectrum below the lower level discriminator.

The TEPC procured for the RaD-X mission is the Environmental Radiation Monitor, Model FWAD-3, Hawk version 3.0, manufactured by Far West Technologies (FWT), Inc., Goleta, CA. The Hawk TEPC is the commercial version of the TEPC developed for the Space Shuttle and the ISS [*Conroy*, 2010] and measures mixed-field radiation environments such as those found in space, at commercial airline altitudes, and in many radiation-producing facilities on Earth. The sensitive volume of the Hawk version 3.0 is a spherical cavity with an inner diameter of 12.57 cm (4.95 inches), which is surrounded by a 0.241 cm tissue-equivalent A-150 plastic wall and filled with tissue-equivalent gas (propane) at a reduced pressure of 7 torr in order to simulate a spherical tissue volume with an effective diameter of 2 μm [*FWT*, 2016]. The vacuum is within an exterior container composed of 0.127 cm thick Al. The TEPC design enables measurement of the energy deposition of charged particles in simulated tissue spheres with dimensions relevant to cells and organelles [*ICRU*, 1983; *Chang and Kim*, 2008]. The charge-produced individual energy deposition events are converted to a voltage pulse and recorded by a 1024-channel multichannel analyzer. This results in a measurement of y,

which is relatable to linear energy transfer (LET), D, quality factor (Q), and H [*ICRU*, 1983; *International Commission on Radiation Units and Measurements (ICRU)*, 1986; *International Commission on Radiological Protection*, 1991]. The y spectrum, D rate, H rate, Q, and dead time are extracted from the Hawk TEPC measurements [*Conroy*, 2010].

The Hawk performs well at dose rates from about 1 μSv/h to about 100 μSv/h. Background significantly affects precision below 1 μSv/h and dead time becomes noticeable above 100 μSv/h. The nominal range of y is from about 0.2 keV/μm to 600 keV/μm [*Caffrey and Hamby*, 2011]. The Hawk encounters noise below 0.2 keV/μm; hence, the lower level discriminator is set not to include pulses in the first two channels, i.e., y below 0.2 keV/μm. Above 600 keV/μm, pulse height saturation can occur in the preamplifier, which would reduce the ability to determine the magnitude of larger energy deposition events.

2.2. Teledyne Total Ionizing Dose (TID) Dosimeter

The instrument used here is the UDOS001 commercial class dosimeter manufactured by Teledyne Microelectronic Technologies (http://www.teledynemicro.com/product/radiation-dosimeter). The TID is a compact hybrid microcircuit that measures energy absorbed in a silicon detector. Ionizing radiation liberates free charge within the silicon detector, and the subsequent current pulses are integrated by the internal microcircuit until the integrated total charge equals a single dose quantum of 0.14 μGy [*Mazur et al*., 2011; *Lindstrom et al*., 2011]. Once this dose quantum is reached, a counter value is incremented.

The TID integrates the dose absorbed by the silicon detector for energy deposits in the nominal range 100 keV to 15 MeV. The detector thickness is 250 μm. Thus, for charged particle transport perpendicularly (straight line) through the detector, the effective LET range in Si would be 0.4–60 keV/μm (for comparison, it should be noted that the LET in tissue would be substantially lower due to differences in densities and other material properties). The stated dose rate rating with associated integrated error of ±20% is 36 μGy/h to 360 mGy/h [*Teledyne Microelectronic Technologies*, 2016].

The Teledyne TID has flown on numerous NASA DC-8 aircraft test flights as part of the Automated Radiation Measurements for Aviation Safety project [*Tobiska et al*., 2015], which is funded by the NASA Small Business Innovation Research Program and led by Space Environments Technologies (spacewx.com). The TID dosimeter has also been operating on board the NASA Lunar Reconnaissance Orbiter since 2009 [*Mazur et al*., 2011].

2.3. Liulin Dosimeter

The instrument used here is the Liulin-6SA1 mobile dosimetry unit, which is manufactured at the Space Research and Technology Institute of the Bulgarian Academy of Sciences in Sofia [*Dachev*, 2009, 2013; *Dachev et al*., 2015]. The Liulin consists of a silicon semiconductor detector, a charge-sensitive preamplifier, and two microcontrollers. Pulse height analysis is used to measure the energy deposition of charged particles in the detector. The amplitude of the pulses after the preamplifier processing is proportional to the energy deposition in the silicon detector and hence to the dose and LET in silicon by the ratio 240 mV/MeV. These amplitudes are digitized by an analog-to-digital converter and arranged in a 256-channel spectrum in order to provide the energy deposition spectrum. The detectable energy range is reported as 0.0813 MeV to 20.8 MeV [*Uchihori et al*., 2002], which would correspond to an effective LET range of 0.27–69.3 keV/um for perpendicular (straight line) transport of charged particles through the 300 μm thick silicon detector. The LET in tissue would be lower. Liulin dosimeters have over a decade of flight heritage on aircraft, balloons, and in space [*Stassinopoulos et al*., 2002; *Spurny and Dachev*, 2003; *Dachev*, 2013; *Dachev et al*., 2015].

2.4. RaySure Dosimeter

RaySure is a compact and lightweight solid-state monitor that uses a single PIN silicon diode to record charge depositions caused by ionizing radiation passing through the sensitive volume. Pulses are binned according to total energy deposited into 15 channels covering a range from 0.1 to 100 MeV. This corresponds approximately to a stopping power in Si of 0.8 to 800 MeV cm^2/g. The geometry of the sensitive volume is a disk with a diameter of 25 mm and a thickness of 500 μm. RaySure is a self-contained and stand-alone monitor that has been extensively flown on commercial and private aircraft and calibrated

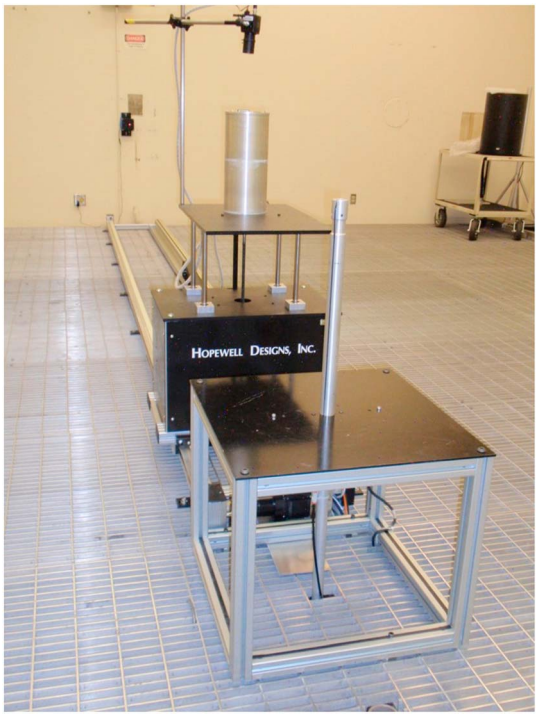

Figure 2. Radiation source exposures at LLNL. A TEPC is seen on the instrument stand. Photograph provided by LLNL.

at various radiation facilities [*Hands and Dyer*, 2009]. For the RaD-X project, RaySure was adapted so that power could be supplied externally from the RaD-X payload platform.

3. Calibration Facility and Sources

3.1. Calibration Facility

A standard radiation calibration facility at the Lawrence Livermore National Laboratory (LLNL) was used to perform the ground-based measurements. This low scatter facility consists of a 12.2 m × 9.1 m × 6 m high concrete shielded room with suspended Al grid flooring to reduce scatter and a heavy shielded interlocked door. The facility was designed to provide precision irradiations for the calibration of personnel dosimeters and environmental dosimeters. To support these operations, the facility maintains a variety of radioactive sources, including gamma and neutron sources. Facility staff operated the sources during our calibrations. We positioned the instruments and acquired the data via our own cables in the control room, or, for the Hawk, data download via removable storage device.

Figure 2 shows detector positioning during irradiation. In this case, a TEPC is seen on the movable table on a rail. The location of the source during irradiation is near the top of the vertical Al tube. A linear positioning system provides accurate positioning of the sources to ±1 mm. A sensor is located at the top of the tube to provide confirmation that the source is in the correct position. The dosimeters were placed one at a time on this movable table at the same height as the source. Source-to-detector distance was then measured and exposure performed. Available distances range from 0.5 m to 5 m. A camera is also seen attached to the movable table that permitted monitoring during irradiation as well as remote readout from instrument panels as needed.

3.2. Calibration Sources

Several NIST-traceable neutron and gamma ray sources are available at the LLNL calibration facility. Based on dose rate and distance considerations, we determined that two sources would be most suitable for calibrating the TEPCs and provide functional tests for the Si dosimeters: a small ^{252}Cf fission source (NS120, 2.04×10^6 neutrons/s) and a small ^{60}Co gamma ray source (400608, 0.0187 Ci). The other sources were determined to provide dose rates substantially above those expected during the RaD-X mission resulting in response saturation (dead time) of the TEPC and were therefore not considered further.

Source-to-detector distances for instrument calibration were selected to ensure robust measurement results with dose rates comparable to those expected during the balloon flight, although the spectra of radiation types and energies will not be comparable. Source-to-detector distances were 100 cm from the ^{252}Cf source and 200 cm from the ^{60}Co source.

4. Facility Standard (Benchmark) Measurements

For comparisons with independent standards, the LLNL calibration facility provided contemporary NIST-traceable measurements for the two sources and distances that we selected. These standard measurements for neutrons and gamma rays are listed in Table 1 and were used here to compare the responses of each instrument. These benchmark measurements were made in June 2015 as described below.

Table 1. Facility Standard (Benchmark) Measurements for the Sources and Distances Used Here[a]

Source	Distance (cm)	D (μGy/h)	H (μSv/h)	$H^*(10)$ (μSv/h)
		Small ^{60}Co		
Gammas	200	32.29 ± 1.61	32.29 ± 1.61	37.45 ± 1.87
		Small ^{252}Cf		
Neutrons	100	2.09 ± 0.21	25.60 ± 2.56	29.78 ± 2.98
Gammas	100	2.49 ± 0.12	2.49 ± 0.12	2.89 ± 0.14
Total	100	4.58 ± 0.51	28.09 ± 3.14	32.68 ± 3.65

[a]Measurements made in June 2015. Values are mean ± SD for dose rates in soft tissue [*ICRU*, 1989]. D is absorbed dose, H is dose equivalent, and $H^*(10)$ is ambient dose equivalent.

The neutron energy spectrum was measured using a Rospec spectrometer [*Bubble Technology Industries*, 2015] at 100 cm from the small ^{252}Cf source 12–15 June 2015. Rospec-associated software was used to unfold the neutron spectrum and calculate the dosimetric quantities. The exposure duration was 238,000 s and was controlled by Rospec's computer with accuracy of ±1 s. The distance from the source was established by the irradiator's control software with accuracy of ±0.1 cm. Alignment of the Rospec spectrometer with the ^{252}Cf source was verified using a laser beam. Per manufacturer, the Rospec energy resolution is $<$10% at 1 MeV, gamma rejection $>$100:1 and nonlinearity $<$0.03%. Neutron background was determined to be negligible and was therefore not accounted for in the neutron benchmark dosimetry. In Table 1, D, H, and $H^*(10)$ are based on the measured neutron spectrum and the appropriate fluence to dose conversion factors [*International Commission on Radiation Units and Measurements*, 1989; *National Council on Radiation Protection and Measurements Report 38*, 1971; *International Commission on Radiological Protection (ICRP)*, 1997].

The gamma ray dose rate contribution from the ^{252}Cf source was measured on 3 June 2015. Measurements were made at 100 cm from the source using an Exradin A6 800 cc ion chamber [*Standard Imaging*, 2008] with Shonka air-equivalent plastic walls (NIST-traceable calibration on 29 October 2014, calibration uncertainty 1.6%) in combination with a Supermax electrometer (NIST-traceable calibration on 28 October 2014, calibration uncertainty 0.2%). NIST-traceable thermometer and barometer were employed. This ion chamber is composed of Teflon and graphite with about 2.5% total hydrogen content. Hence, the neutron response is low; our estimate is not more than 5% of the gamma ray dose rate. Five successive measurements were made and the mean ± SD calculated. The measurement time for each of the five measurements was 300 s. The electrometer was zeroed between measurements to minimize the effect of leakage current on the results. The ion chamber was allowed to stabilize prior to initiating each measurement.

The gamma ray dose rate from the ^{60}Co source was measured on 3 June 2015. In this case, measurements were made at 200 cm from the source using the Exradin A6 800 cc ion chamber. Five successive measurements were made and results were averaged and SD was calculated. The measurement time for each of the five successive measurements was 120 s. Otherwise, the same procedures were employed as described above for ^{252}Cf gamma rays. Measurements were corrected for background, temperature, and barometric pressure.

Table 2. Calibration Measurements for TEPCs

Source	Distance (cm)	D_{A150} Rate (μGy/h)	D Rate (μGy/h)[a]	H Rate (μSv/h)[a]	$H^*(10)$ Rate (μSv/h)[a]
		TEPC #32 (Flight Unit) Measured on 11 August 2014			
Bkg	–	0.43 ± 0.07	0.43 ± 0.07	0.44 ± 0.07	–
Small ^{60}Co	200	30.10 ± 1.51	30.14 ± 1.51	30.20 ± 1.51	35.03 ± 1.75
Small ^{252}Cf	100	5.09 ± 0.57	5.10 ± 0.57	29.71 ± 3.32	34.46 ± 3.85
		TEPC #33 (Ground Unit) Measured on 15 January 2015			
Bkg	–	0.32 ± 0.09	0.32 ± 0.09	0.35 ± 0.10	–
Small ^{60}Co	200	26.42 ± 0.35	26.46 ± 0.35	26.47 ± 0.36	30.71 ± 0.42
Small ^{252}Cf	100	4.83 ± 0.45	4.84 ± 0.45	28.29 ± 2.64	32.82 ± 3.06

[a]For *ICRU* [1989] soft tissue using mass energy absorption coefficients in Table 3 and corrected for background and dead time. $H = D \times Q$, where Q was obtained from the measured y spectrum for both neutrons and gammas (see Figure A2). $H^*(10) = H \times 1.16$ [*ICRP*, 1997].

Table 3. Mass Energy Absorption Coefficients[a]

Material	^{60}Co Gamma Rays μ_{en}/ρ (cm^2/g)	^{252}Cf Gamma Rays μ_{en}/ρ (cm^2/g)
A-150	0.02934	0.03172
Si	0.02652	0.02875
ICRU-44 Soft Tissue	0.02938	0.03176

[a]From *NIST* [2016].

5. Dosimeter Measurements

5.1. TEPCs

Calibration measurements for two TEPCs are listed in Table 2. TEPC #32 was included on the balloon flight and #33 remained on the ground, although TEPC #33 was on board a supporting aircraft flight [see *Mertens et al*., 2016].

The TEPCs provide reproducible results for both background and source-and-distance-specific measurements. At 200 cm from the small ^{60}Co gamma ray source, both TEPCs provide SDs of about 5% of the mean. At 100 cm from the ^{252}Cf source, the SDs are larger (about 10% of the mean). Larger SDs were expected for ^{252}Cf due to the dose being delivered by a smaller number of large energy deposition events relative to those produced by the ^{60}Co source. Also, the TEPC performs consecutive 1 min measurements, which are averaged over the exposure duration (typically 30 min or more). Therefore, the SDs are also influenced by the exposure duration (the number of 1 min measurements).

It is noted in Table 2 that TEPC #33 has somewhat lower response than TEPC #32. However, these measurements were conducted about 5 months apart. When the TEPC #32 measurements on 11 August 2014 are adjusted to account for radioactive decay of the sources to 15 January 2015 (the date of the TEPC #33 measurements), the comparisons are 28.45 ± 1.42 μGy/h for ^{60}Co gamma rays and 4.68 ± 0.52 μGy/h for ^{252}Cf radiation. These results do not differ significantly from the TEPC #33 measurements of 26.42 ± 1.32 μGy/h for ^{60}Co gamma rays and 4.83 ± 0.45 μGy/h for ^{252}Cf radiation. The difference observed in the background measurements is likely due to background variations on different times of the year. Note that the final calibrations and dosimeter intercomparisons are based on TEPC #32, which was the flight unit.

The proton drop points for both Hawks were determined using ^{252}Cf prior to final calibration to verify that the instruments were operating properly. Both demonstrated proton drop points at y of about 150 keV/μm, which is consistent with the expectation for the TEPC and provides added assurance that the TEPCs were functioning properly.

Measurement results for the TEPCs were converted from the absorbed dose in A150 plastic to absorbed dose in soft tissue using ratio of mass energy absorption coefficients listed in Table 3 (obtained from *National Institute of Standards and Technology (NIST)* [2016]). For ^{60}Co gamma rays, we used 1.25 MeV mean energy and for ^{252}Cf gamma rays we used 0.8 MeV mean energy [*Billnert et al*., 2013]. As seen in Table 2, the differences in D rates for A150 plastic and soft tissue are negligible.

Table 4. Measurements With Shielding at 100 cm From the Small ^{252}Cf Source[a]

Shielding	D_{total} (μGy/h)	D_{gamma} (μGy/h)[b]	$D_{neutron}$ (μGy/h)
Background (no source)	0.286 ± 0.058	0.280 ± 0.062	–
^{252}Cf and no shielding	4.708 ± 0.353	2.292 ± 0.214	2.416 ± 0.289
^{252}Cf and 5.08 cm poly	4.814 ± 0.384	2.237 ± 0.205	2.577 ± 0.313
^{252}Cf and 0.3175 cm Al	4.700 ± 0.458	2.212 ± 0.228	2.488 ± 0.353
^{252}Cf and 0.9525 cm Al	4.373 ± 0.472	2.011 ± 0.231	2.362 ± 0.372
^{252}Cf and 1.270 cm Al	4.176 ± 0.345	1.969 ± 0.173	2.207 ± 0.266
^{252}Cf and 1.270 cm Al + 5.08 cm poly	4.284 ± 0.433	1.961 ± 0.205	2.323 ± 0.338
Background (no source)	0.310 ± 0.078	0.287 ± 0.078	–

[a]On 5 March 2015. TEPC #33 (the ground-based unit) was used for these measurements. These results have not been converted to soft tissue.
[b]Obtained for gamma cutoff at $y < 13.5$ keV/μm.

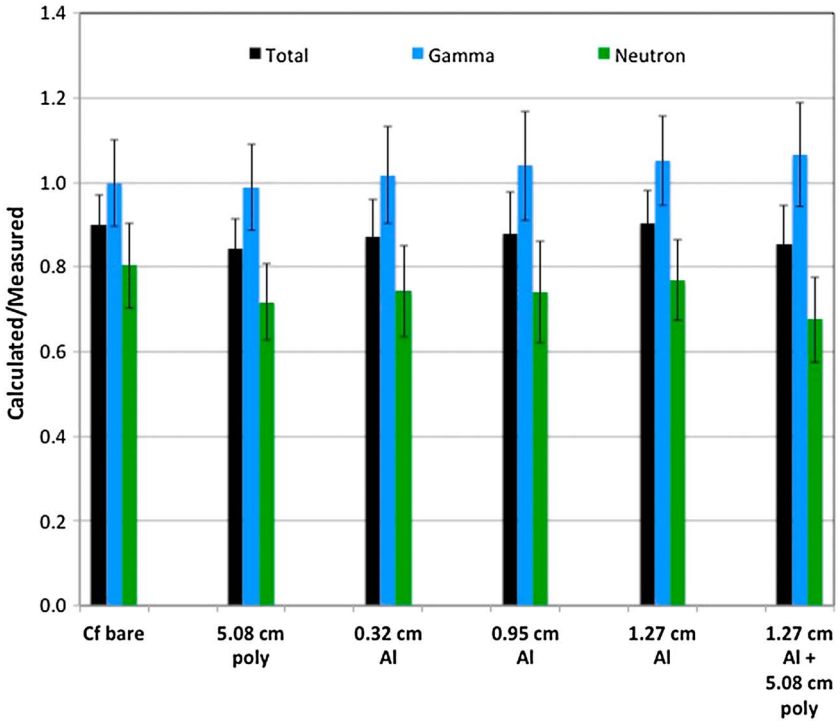

Figure 3. Comparison of the measured results in Table 4 with the preliminary modeling calculations in *Gronoff et al.* [2016]. Error bars are ± SD.

TEPC measurements at 100 cm from the small ^{252}Cf source were also performed at LLNL with intervening Al and polystyrene shields to provide data for evaluating the radiation-modeling codes used to help interpret the in-flight measurements (for modeling results see *Gronoff et al*. [2016]). The flight package was composed of an Al outer container with thickness of 0.635 cm on the sides, 1.25 cm on the bottom, and 0.9525 cm on the top, with an additional 5.08 cm polyethylene surrounding the detectors.

The TEPC measurement results are provided in Table 4. It is observed that these materials and thicknesses do not appreciably influence *D* rate from ^{252}Cf radiation, albeit some (~10%) dose rate reduction is suggested for both gamma rays and neutrons with the thickest Al shields.

Comparing the measured results with preliminary modeling calculations in Figure 3 shows that the gamma ray dose rate contribution is calculated within the measurement uncertainties. However, the calculations for neutrons are consistently lower than the measurements by 20 to 30%. We expect the agreement between calculated and measured dose rates for neutrons will improve as the modeling work continues [*Gronoff et al*., 2016].

It is also noted that when the measured dose rates are adjusted to account for radioactive decay of the ^{252}Cf source between 5 March 2015 and 12 June 2015 (the benchmark date), the results in Table 4 for ^{252}Cf at 100 cm with no shielding produced *D* rates of 4.47 ± 0.34 μGy/h total, 2.17 ± 0.20 μGy/h gamma, and 2.29 ± 0.27 μGy/h neutron. These compare well with the results in Table 1 for the benchmark measurements and the results in Table 2 for the TEPC. Again, confirming the reproducibility of the TEPCs.

5.2. TID

Results for the Teledyne TID dosimeter are listed in Table 5. These measurements were conducted on 12 August 2014. The mean absorbed dose rate measured at 200 cm from the ^{60}Co source was 35.19 ± 10.21 μGy/h. Subtracting a background of 0.42 μGy/h (obtained as described below) results in 34.77 ± 10.08 μGy/h. This does not differ significantly from the results observed with the TEPCs at 200 cm from the ^{60}Co source. However, the uncertainty associated with the TID measurement is substantially larger than observed for the TEPCs.

Table 5. Calibration Measurements for the Teledyne TID on 12 August 2014[a]

Source	Distance (cm)	$D_{Silicon}$ μGy/h	D_{Tissue} μGy/h
Bkg	–	~0.42	–
Small ^{60}Co	200	34.77 ± 10.08	38.52 ± 11.17
Small ^{252}Cf	100	2.69 ± 0.83	2.97 ± 0.92

[a]An estimated background of 0.42 has been subtracted from the ^{60}Co and ^{252}Cf measurements, estimated as described in text. Conversion from absorbed dose measured in Si to absorbed dose in soft tissue was performed using ratio of mass energy absorption coefficients from Table 3.

The uncertainties associated with the TID detector are twofold: difficulties associated with measuring background *and* sampling uncertainties associated with the quantum steps. The TID increments 0.14 μGy of dose in quantum steps and the low-level output increments 19.5 mV each time the detector registers a quantum step. In a low dose rate background environment, it can take hours before the output registers an increment. Hence, the background level at ground-based facilities is difficult to measure using the TID. Under conditions where exposures are integrated over a relatively brief period of time (e.g., at a calibration facility), dose rates are obtained by computing a numerical derivative from the time series of accumulated dose, which must be sampled at a finite rate. The difficulty is that one can never catch the time increment exactly, which introduces a sampling uncertainty into the calculation of the dose rate. Also, during the LLNL measurements we discovered that the low-level output pin is noisy adding substantially to the uncertainty associated with the TID dosimeter. Hence, our best estimate SD for the TID is about ±30%. It is possible (likely) that these uncertainties would be smaller for applications involving continuous in-flight measurements because sampling errors would be less important for long duration integrated measurements.

Also, the TID provides lower response to ^{252}Cf radiation than the TEPC. At 100 cm from the ^{252}Cf source the dose rate measured with the TID is 3.11 ± 0.96 μGy/h. Subtracting the background of 0.42 μGy/h results in a net measurement of 2.69 ± 0.83 μGy/h in Si, which converts (as described below) to 2.97 ± 0.92 μGy/h in soft tissue. For comparison, the TEPC measured 5.09 ± 0.57 μGy/h on 11 August 2014.

TID measurement results were converted from absorbed dose in Si to absorbed dose in International Commission on Radiation Units and Measurements (ICRU) soft tissue using the ratio of mass energy absorption coefficients (Table 3). A mean energy of 1.25 MeV was used for ^{60}Co gamma rays and a mean energy of 0.8 MeV was used for ^{252}Cf gamma rays [*Billnert et al*., 2013]. Any possible neutron response in the Si was not considered when converting the ^{252}Cf measurements to soft tissue.

As discussed above, the response of the TID dosimeter to background (no source) could not be measured. The background response was therefore estimated here by scaling to Liulin, which is also a Si-based sensor. However, even if this background estimate is incorrect by a factor of 2, it would not significantly impact our interpretation of the ^{60}Co gamma ray results but could have a larger impact on the ^{252}Cf results.

5.3. Liulin

Results for the Liulin dosimeter are listed in Table 6. These measurements were conducted on August 11, 2014. The mean absorbed dose rate measured at 200 cm from the ^{60}Co source was 42.98 ± 0.85 μGy/h. Subtracting a background of 0.52 ± 0.12 μGy/h results in 42.46 ± 0.86 μGy/h. Converting this measurement in Si to absorbed dose in ICRU soft tissue results in 47.04 ± 0.93 μGy/h. This is substantially higher than observed with TEPC #32 on the same date of 30.14 ± 1.51 μGy/h and is clearly outside the apparent statistical variability of these instruments. It should be noted that the large overresponse of the Liulin observed during ground-based exposure to ^{60}Co gamma rays was also seen in flight (see Table 9 and section 7) which indicates that *this* Liulin has a substantial overresponse to low LET radiation. It is also noteworthy that the low LET component of the spectrum in flight appears to be consistent with the Compton spectrum from ^{60}Co gamma rays, which may explain the reason for the similar overresponse (section 7).

For ^{252}Cf radiation, the Liulin provides substantially lower response than the TEPC. At 100 cm from the source, the Liulin measured 3.35 ± 0.27 μGy/h. Subtracting a background of 0.52 ± 0.12 μGy/h results in

Table 6. Calibration Measurements for the Liulin on 11 August 2014[a]

Source	Distance (cm)	$D_{Silicon}$ μGy/h	D_{Tissue} μGy/h [b]
Bkg	–	0.52 ± 0.12	–
Small ^{60}Co	200	42.46 ± 0.86	47.04 ± 0.93
Small ^{252}Cf	100	2.83 ± 0.25	3.14 ± 0.28

[a]Background has been subtracted.
[b]Conversion from absorbed dose measured in Si to absorbed dose in soft tissue performed using ratio of mass energy absorption coefficients (see Table 3).

an absorbed dose rate in Si of 2.83 ± 0.25 μGy/h. Converting to absorbed dose rate in ICRU soft tissue results in 3.14 ± 0.28 μGy/h. This is lower than observed with the TEPC of 5.09 ± 0.57 μGy/h measured on the same date.

5.4. RaySure

Calibration measurements for the RaySure dosimeter are listed in Table 7. These measurements were conducted on 11 August 2014. The mean absorbed dose rate measured at 200 cm from the ^{60}Co gamma ray source was 26.94 ± 6.3 μGy/h. Subtracting a background of 0.24 ± 0.09 μGy/h results in 26.7 ± 6.3 μGy/h. Converting to absorbed dose rate in ICRU soft tissue results in 29.6 ± 7.0 μGy/h. This does not differ significantly from that observed with TEPC #32 on the same date of 30.14 ± 0.33 μGy/h, albeit the measurement uncertainty is larger for the RaySure because it includes a systematic uncertainty related to the width of the energy deposition channels. We believe this is quite conservative but justified.

For ^{252}Cf radiation, the RaySure provides substantially lower response than the TEPCs. At 100 cm from the source, the RaySure measured 1.6 ± 0.5 μGy/h, which is substantially lower than the TEPC and also lower than observed for the other two Si-based dosimeters. The difference between the Si-based detectors is likely due to detection thresholds. RaySure has a high detection threshold of 100 keV because it has a large sensitive area. Both the gammas and neutrons from ^{252}Cf impart only a fraction of their (already low) energy to the silicon and hence both will be undermeasured by RaySure. It is noted that RaySure correctly measured the ^{60}Co gamma ray dose as seen in Table 8. Hence, only the ^{60}Co gamma ray results were converted to dose in tissue (Table 7) using the ratio of mass energy absorption coefficients (Table 3). The results for ^{252}Cf radiation are considered too uncertain as the RaySure response to the full spectrum of radiations emitted by ^{252}Cf has not yet been adequately determined. It should be noted that measurements of higher-energy monoenergetic neutrons (3 MeV d-D and 14 MeV d-T) are consistent with simulations suggesting that the lower than expected response to ^{252}Cf may result from the lower energy components of the ^{252}Cf fission spectrum, either neutrons, gammas, or both. Due to its relatively high minimum energy deposition threshold, RaySure is not well suited to, and was not designed for, such a low-energy environment. However, in the higher-energy atmospheric radiation environment, comparisons between RaySure and TEPC data are far more favorable. This is discussed further in a companion paper [*Hands et al.*, 2016].

6. Comparisons With Benchmark

The dosimeter calibration measurements are compared with the facility benchmark measurements in Table 8. For intercomparison, our dosimeter results were adjusted for radioactive decay to coincide

Table 7. Calibration Measurements for the RaySure on 11 August 2014[a]

Source	Distance (cm)	$D_{Silicon}$ μGy/h	D_{Tissue} μGy/h
Bkg	–	0.24 ± 0.09	–
Small ^{60}Co	200	26.7 ± 6.3	29.6 ± 7.0
Small ^{252}Cf	100	1.6 ± 0.5	na[b]

[a]Background has been subtracted. Conversion from absorbed dose measured in Si to absorbed dose in soft tissue was performed using ratio of mass energy absorption coefficients in Table 3.
[b]For ^{252}Cf radiation, the conversion to D_{Tissue} is not considered meaningful as described in text.

Table 8. Dosimeter Comparisons With Benchmark[a]

Source	LLNL Benchmark	TEPC #32	TID	Liulin	RaySure
Absorbed Dose Rate (μGy/hr)					
^{60}Co Gammas	32.29±1.61	27.09±1.35	34.64±10.04	42.28±0.84	26.59±6.27
^{252}Cf Neutrons	2.09±0.21	2.10±0.21	na	na	na
^{252}Cf Gammas	2.49±0.12	2.23±0.11	na	na	na
^{252}Cf Total	4.58±0.51	4.32±0.48	2.53±0.78	2.66±0.22	1.5±0.5
Dosimeter-to-Benchmark Ratios					
^{60}Co Gammas	1.00±0.05	0.84±0.06	1.07±0.32	1.31±0.07	0.82±0.20
^{252}Cf Neutrons	1.00±0.10	1.00±0.14	na	na	na
^{252}Cf Gammas	1.00±0.05	0.90±0.06	na	na	na
^{252}Cf Total	1.00±0.11	0.94±0.15	0.55±0.18	0.58±0.08	0.33±0.12

[a]Dosimeter results were adjusted to account for radioactive decay of the sources from the measurement date to the benchmark date. Absorbed dose (D) based on soft tissue (ICRU 1989). Uncertainties are ±SD.

with the benchmark measurement dates. For ^{60}Co the adjustment was straightforward using the half-life of 5.27 years. However, for Cf the changing half-life with the age of the source required determination of a half-life suitable for the period between the calibration measurements and the benchmark measurements, i.e., during the period between August 2014 and June 2015. For this period, the best estimate half-life for the small Cf source is 3.55 years. The changing (increasing) half-life with time for this Cf source is illustrated in Figure A2. The source was 30.79 years old in 12 June 2015, and Figure A2 shows that only three isotopes contributed significantly to the neutron emission rate at that time, i.e., ^{250}Cf (28%), ^{252}Cf (67%), and ^{248}Cm (5%).

Table 8 provides intercomparisons of *D* rates based on absorption in soft tissue. It is observed that for ^{60}Co gamma rays, the TEPC, TID, and RaySure compare reasonably well with the benchmark. The Liulin responds higher than the benchmark measurement and the other dosimeters.

For ^{252}Cf radiation, the TEPC is in excellent agreement with the benchmark, i.e., does not differ significantly. The gamma *D* rate was obtained for the TEPC by evaluating the *y* spectrum below 13.5 keV/μm and the neutron *D* rate was obtained by subtracting the gamma *D* rate from the total measured *D* rate.

It is seen in Table 8 that the Si-based dosimeters (TID, Liulin, and RaySure) underrespond to the ^{252}Cf radiation. The total *D* rate from ^{252}Cf measured by the TID and Liulin appears to agree with the ^{252}Cf gamma ray *D* rate only. The RaySure response to Cf radiation is lower than observed for the TID and Liulin (see section 5.4 for a discussion on the RaySure response). Based on these measurements, it is not clear whether this is due to low sensitivity to neutrons by the Si detectors, some other response relationship peculiar to the mixed neutron/gamma ^{252}Cf radiation, or a combination of these.

Table 8 also provides dosimeter-to-benchmark ratios for the four flight dosimeters. For ^{60}Co gamma rays, the means for the TEPC, TID, and RaySure are −16%, +7%, and −18% compared with the benchmark, respectively. The 16% underresponse of the TEPC is most likely due to the *y* distribution of ^{60}Co gamma rays extending to the lower channels where the lower level discriminator (LLD) is used to limit noise. The LLD was set to eliminate pulses in the first two channels ($y = 0$–0.1 and 0.1–0.2 keV/μm), which would contain some pulses from the higher-energy portion of Compton electrons produced by ^{60}Co gamma ray interactions in the detector. The mean for Liulin is 31% higher than the benchmark, which is not explainable based on the measurement SDs, but appears to be reproducible with this Liulin dosimeter as it was also observed in flight (see section 7 and Table 9).

For ^{252}Cf radiation, only the TEPC provides results comparable to the benchmark. The dose rates measured with the TEPC do not differ significantly from the LLNL benchmark measurements.

Dosimeter-to-benchmark ratios for *H* and *H**(10) were also obtained (not listed in Table 8). For intercomparison, our dosimeter results were adjusted to account for radioactive decay to coincide with the benchmark measurement dates. For ^{60}Co gamma rays, the dosimeter-to-benchmark ratios for *H* and *H**(10) are essentially identical to those obtained for *D* in Table 8 because $Q = 1$ and a constant factor of 1.16 [*ICRP*, 1997] is used to convert from *H* to *H**(10).

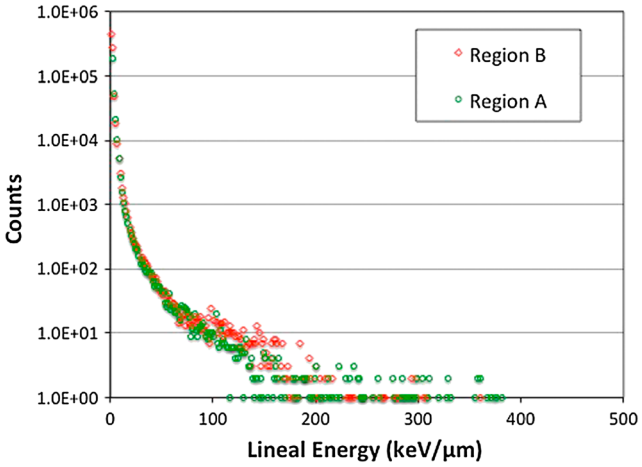

Figure 4. Lineal energy spectra measured by the TEPC at mean barometric altitudes of 24.3 km (Region A, 30 g/cm^2) and 36.7 km (Region B, 5 g/cm^2) during the RaD-X balloon flight.

For ^{252}Cf radiation, dosimeter-to-benchmark H and $H^*(10)$ ratios could only be obtained for the TEPC. Although the Si-based dosimeters provide total measured response from the ^{252}Cf radiation (neutrons plus gammas), they do not provide separate neutron and gamma dose rate information or neutron Q information and therefore could not be used to determine H and $H^*(10)$ from these calibration measurements. The H and $H^*(10)$ obtained from the TEPC results do not differ significantly from the benchmark values for ^{252}Cf radiation, i.e., TEPC-to-benchmark ratio of 0.90 ± 0.14.

7. Initial Evaluation of Flight Results Based On the TEPC Data

As discussed in section 2.1, a ground-based calibrated TEPC served as the "flight standard" and provided a means to interpret the TEPC measurements in flight, as well as a way to compare responses from the Si-based dosimeters in flight with a calibrated in-flight standard, recognizing that there are limitations to such comparisons. Here we provide some examples of how the results from the calibrated TEPC can be used to analyze the flight data. More extensive results and discussion of the flight data are presented in companion papers in this special issue [*Mertens et al.*, 2016; *Hands et al.*, 2016; *Gronoff et al.*, 2016] and will also be provided in follow-on publications as the flight data are analyzed further.

Lineal energy spectra measured during flight by the TEPC are shown in Figure 4 for two barometric altitudes. Region A is at a barometric altitude range of 21–27 km (24.3 km mean) and Region B is at >32 km (36.7 km mean). These spectra were obtained at low gain, which permits observation of y from the high-LET components of the radiation field.

It is observed that the lineal energy spectra in Figure 4 are similar for the two altitudes at y less than about 75 keV/μm, but region B has substantially more counts at larger y. This can be seen more clearly when plotting the ratio of B/A against y (Figure 5). The ratio of counts is close to unity below about 75 keV/μm. The additional counts above 100 keV/μm in Region B compared with Region A is also observed in Figure 14 of *Mertens et al.* [2016]. These observations are consistent with results in Figure 12 of *Reitz* [1993] demonstrating that the flux from heavy ions (Z = 6 to 28) is strongly dependent on atmospheric depth at the altitudes considered here, and we should therefore expect more large y events in B (atmospheric depth 5 g/cm^2) than in A (30 g/cm^2).

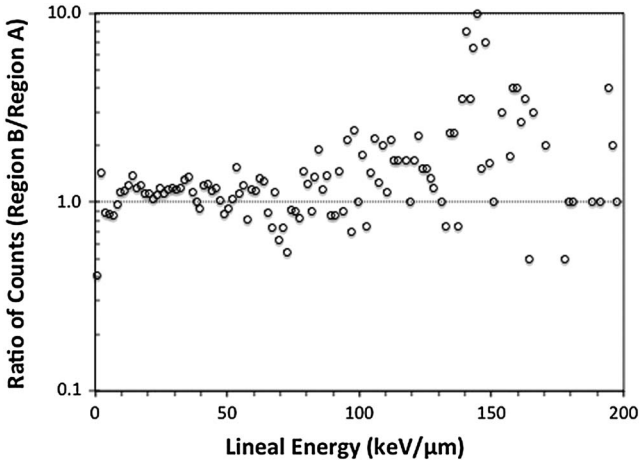

Figure 5. Ratio of counts (Region B/Region A) as a function of lineal energy measured by the TEPC.

The low LET response (obtained at high gain) is illustrated in Figure 6a. Here we plot the y spectra below 10 keV/μm for regions A and B and

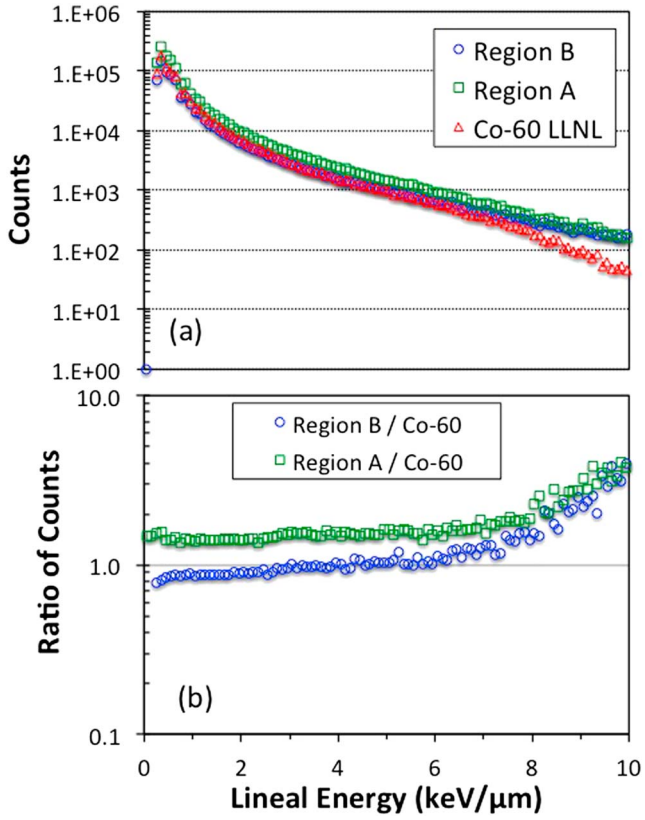

Figure 6. (a) Lineal energy distributions measured with the TEPC at barometric altitudes of 24.3 km (Region A) and 36.7 km (Region B) during the RaD-X balloon flight. These are low LET spectra from high-gain data acquisition. The *y* spectrum measured with the same TEPC at LLNL for ^{60}Co gamma rays is included for comparison. (b) Ratio of counts for results in Figure 6a, i.e., counts measured in-flight in Regions A and B divided by the counts obtained for ^{60}Co gamma rays.

compare them with the *y* spectrum for ^{60}Co gamma rays measured at LLNL during our calibrations of the same TEPC. It is observed that regions A and B provide similar *y* spectra in the low LET region, albeit region A exhibits somewhat more low LET events.

Interestingly, it is observed that the *y* spectrum measured for ^{60}Co gamma rays is similar to those observed in both Regions A and B below about 7 keV/μm, which would include most *y* values associated with the Compton electrons from ^{60}Co gamma rays.

This can be seen more clearly in Figure 6b. Here the *y* spectra measured in flight using TEPC #32 at two altitudes are compared with the *y* spectrum for ^{60}Co gamma rays measured using TEPC #32 on the ground. Ratios are counts measured in flight in regions A and B divided by counts measured with ^{60}Co gamma rays on the ground. Although there are more low LET events in Region A than in B, the ratios are nearly constant below about 7 keV/μm at both altitudes suggesting that Compton electrons produced by ^{60}Co gamma rays may be a reasonable proxy for the low LET component encountered at these altitudes.

Dose rates measured in flight with the TEPC in Regions A and B are compared in Table 9 with those obtained from the Liulin dosimeter. It is observed that the Liulin overresponds at all three altitudes. Also, the overresponse is consistent with that observed during ground-based calibrations to ^{60}Co gamma rays (Table 8). This suggests that the high response of the Liulin observed during ground-based calibrations was real and reproducible and continued during the flight measurements. It is not clear, however, whether this is an inherent problem with the Liulin or this resulted from problems with this particular device during the measurement campaign. More comparisons of the dosimetry results during flight are provided in *Mertens et al.* [2016]; additional refinements and interpretations are expected as the data are analyzed further.

8. Conclusions

Four dosimeters on the RaD-X balloon flight mission, and one on the ground, were evaluated at LLNL using NIST-traceable ^{60}Co and ^{252}Cf radiation sources. Although these sources do not simulate the radiation environment in the stratosphere, they are appropriate for calibration of the TEPC and provide functional tests for the Si based dosimeters. Standard "benchmark" measurements were also performed contemporaneously for these sources by LLNL calibration facility personnel at the same positions and distances used to evaluate the dosimeters.

For ^{60}Co gamma rays, comparisons with the benchmark determined that the means obtained for the TEPC, TID, Liulin, and RaySure were −16%, +7%, +31%, and −18% of the benchmark, respectively.

Table 9. Comparison of Flight Results for TEPC and Liulin Dosimeters

Barometric Altitude (km)	TEPC (μGy/h)	Liulin[a] (μGy/h)	Liulin/TEPC
8	0.90	1.25	1.39
24.3	3.20	4.44	1.39
36.7	2.73	3.68	1.35

[a]Converted from dose rate in Si to water equivalent using multiplicative ratio of 1.33 for GCR spectrum [*Schwadron et al.*, 2012].

Except for the Liulin, the dosimeters agreed reasonably well with each other and with the benchmark. The 31% overresponse to ^{60}Co gamma rays observed with the Liulin is substantially larger than can be explained based on the standard deviation of the measurements (the overresponse was also observed in flight, see below).

For ^{252}Cf radiation, only the TEPC results were in agreement with the benchmark. The three Si detectors substantially underresponded to the ^{252}Cf radiation. The reason for the underresponse is not clear from these calibration measurements and may be unique to each dosimeter based on their particular design and performance characteristics. The low hydrogen content of the Si detectors also influences their sensitivity to the neutron component of the ^{252}Cf radiation.

TEPC-based evaluations of flight data show larger average LET (more large y events) at 36.7 km than at 24.3 km. Based on available published data, the additional large y events at 36.7 km (Region B) compared with 24.3 km (Region A) are expected to be primarily from heavy ions ($Z = 6$–28). Modeling is underway to characterize the RaD-X radiation environment.

Comparing the y distribution measured with the TEPC for ^{60}Co gamma rays with those obtained with the same TEPC in flight suggests that the Compton electrons produced by ^{60}Co gamma rays may be a reasonable proxy for the low LET radiation component encountered in the stratosphere. This could be useful information for ground-based calibration.

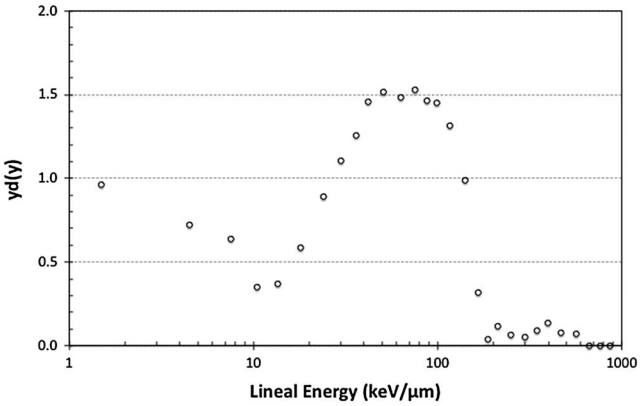

Figure A1. Lineal energy (y) spectrum for ^{252}Cf measured with the TEPC at 100 cm from the small ^{252}Cf source. The ordinate axis is the product of y and d(y), i.e., the fraction of dose delivered between y and $y + dy$. It is observed that the ^{252}Cf fission neutrons contribute to yd(y), and therefore to the neutron dose rate, between lineal energies of about 13.5 keV/μm and 150 keV/μm. Below about 10 keV/μm the ^{252}Cf fission gamma rays together with gamma rays produced in the air and in the heavy room shielding dominate. A sharp decline in yd(y) is observed at about 150 keV/μm. This is the "proton drop point," which occurs at about 150 keV/μm regardless of the incident neutron energy and is therefore used in the calibration of the TEPC. The few events above 150 keV/μm are primarily due to carbon recoil nuclei.

Finally, the flight results permitted evaluation of the overresponse observed for the Liulin during the ground-based exposures. The overresponse was observed in flight as well indicating that this instrument responds about 30% too high to low LET radiation, in this case to ^{60}Co gamma rays and to the low LET component of the radiation environment in the stratosphere, which provide similar y spectra in the Compton region and could therefore possibly explain the similar overresponses observed on the ground and in the stratosphere.

Appendix A

Provided in Appendix A are a y spectrum measured with the TEPC at 100 cm from the small Cf source at LLNL (Figure A1) and the isotope-specific neutron emission rates as a function of time since this source was produced (Figure A2).

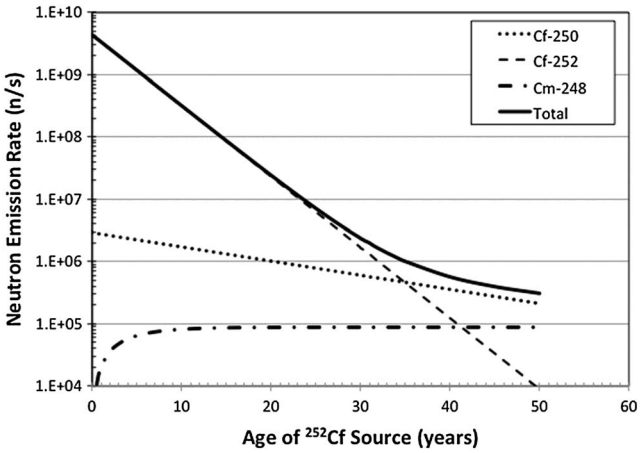

Figure A2. Neutron emission from the small LLNL ^{252}Cf source (NS-120). The source was almost 31 years old in June 2015, the time of the LLNL benchmark measurements. Neutron emission rates as a function of time were calculated for long half-life nuclides from the known isotopic content of the source on 5 September 1984 and accounting for the production of ^{248}Cm from the radioactive decay of ^{252}Cf.

Acknowledgments

The authors thank the Lawrence Livermore National Laboratory for letting us use their calibration facility. We are grateful to William Carl for his invaluable help in making these measurements possible by so generously providing his time and information about LLNL sources and operating the sources as well as his benchmark measurements of the gamma ray dose rates from the ^{60}Co and ^{252}Cf sources. We are also grateful to Radoslav Radev for his benchmark neutron measurements of the ^{252}Cf source, which provided the neutron energy spectrum, the neutron tissue-kerma (*D*) rate, the neutron dose-equivalent (*H*) rate, and the ambient neutron dose-equivalent [*H**(10)] rate. We also thank Richard Wilkins for helping with the RaySure and James Rosenthal for his help with the Teledyne dosimeter during the LLNL calibrations. The author (TS) thanks Leslie Braby for his very helpful comments and suggestions during the preparation of this manuscript. We acknowledge the support from the NASA Langley Research Center, which provided civil servant labor costs for the Langley participants and contributed to costs associated with the LLNL calibration facility and travel for those participating in the dosimeter calibration campaign. The Langley Science Directorate contributed to the procurement of the science instruments. We also acknowledge the support from the NASA Ames Research Center, Space Biosciences Division, and the NASA Ames Science Director, Michael Bicay, who enthusiastically supported this effort. The authors acknowledge the support from the NASA Science Mission Directorate under the Hands-On Project Experience (HOPE-4) opportunity, which was the principal source of funding for the RaD-X balloon flight mission. Data supporting the results in this paper may be obtained by contacting Straume.

References

Badhwar, G. D., et al. (1996), In-flight radiation measurements on STS-60, *Radiat. Meas.*, *26*(1), 17–34.

Billnert, R., F. J. Hambsch, A. Oberstedt, and S. Oberstedt (2013), New prompt spectral gamma-ray data from the reaction ^{252}Cf(sf) and its implication on present evaluated nuclear data files, *Phys. Rev.*, *C87*, 024,601, doi:10.1103/PhysRevC.87.024601.

Bubble Technology Industries (2015), Bubble Technology Industries. 31278 Highway 17, P.O. Box 100 Chalk River, Ontario, Canada K0J 1J0. [Available at http://bubbletech.ca/product/rospec/, accessed October 31, 2015.]

Caffrey, J. A., and D. M. Hamby (2011), A review of instruments and methods for dosimetry in space, *Adv. Space Res.*, *47*, 563–574.

Chang, S.-Y., and B.-H. Kim (2008), Understanding of the microdosimetric quantities obtained by a TEPC, *J. Nucl. Sci. Tech. Suppl.*, *5*, 213–216.

Conroy, T. (2010), Hybrid pulse height/integration analysis method for portable TEPC instrument. In: International Workshop on Real Time Measurements, Instrumentation & Control, IEEE NPSS, Toronto.

Dachev, T. P. (2009), Characterization of the near Earth radiation environment by Liulin type spectrometers, *Adv. Space Res.*, *44*, 1441–1449.

Dachev, T. P. (2013), Profile of the ionization radiation exposure between the Earth surface and free space, *J. Atmos. Sol. Terr. Phys.*, *102*, 148–156.

Dachev, T. P., et al. (2015), Overview of the Liulin type instruments for space radiation measurement and their scientific results, *Life Sci. Space Res.*, doi:10.1016/j.lssr.2015.01.005.

Far West Technologies (FWT) (2016), Far West Technology, Inc. [Available at http://www.fwt.com/detector/fw-ad1ds.htm, accessed February 2016.]

Gersey, B. B., T. B. Borak, S. B. Guetersloh, C. Zeitlin, J. Miller, L. Heilbronn, T. Murakami, and Y. Iwata (2002), The response of a spherical tissue equivalent proportional counter to iron particles from 200–1000 MeV/nucleon, *Radiat. Res.*, *157*, 350–360.

Gronoff, G., C. J. Mertens, R. B. Norman, T. Straume, and T. C. Lusby (2016), Assessment of the influence of the RaD-X balloon payload on the onboard radiation detectors, *Space Weather*, doi:10.1002/2016SW001405.

Hands, A., and C. Dyer (2009), Technique for measuring dose equivalent and neutron fluxes in radiation environments using silicon diodes, *IEEE Trans. Nucl. Sci.*, *56*, 3442–3449.

Hands, A., et al. (2016), The disappearance of the Pfotzer-Regener maximum in dose equivalent measurements in the stratosphere, *Space Weather*, doi:10.1002/2016SW001402.

International Commission on Radiological Protection (1991), *1990 Recommendations of the International Commission on Radiological Protection*, *Publication 60, Annals of the ICRP 21(1–3)*, Pergamon Press, Oxford.

International Commission on Radiological Protection (ICRP) (1997), *Conversion Coefficients for use in Radiological Protection against External Radiation*, *ICRP Publication 74, Annals of the ICRP 26(3/4)*, Pergamon Press, Oxford.

International Commission on Radiation Units and Measurements (ICRU) (1983), Microdosimetry. Report 36, International Commission on Radiation Units and Measurements, Bethesda, Md.

International Commission on Radiation Units and Measurements (ICRU) (1986), The quality factor in radiation protection, International Commission on Radiation Units and Measurements, ICRU Report 40, Bethesda, Md.

International Commission on Radiation Units and Measurements (1989), Tissue substitutes in radiation dosimetry and measurements, International Commission on Radiation Units and Measurements, ICRU Report 44, Bethesda, Md.

Langhoff, S. R., and T. Straume (2012), Space Weather Risks and Society, *Space Weather*, *10*, S06004, doi:10.1029/2012SW000792.

Lindborg, L., and H. Nikjoo (2011), Microdosimetry and radiation quality determinations in radiation protection and radiation therapy, *Radiat. Prot. Dosim.*, *143*(2–4), 402–408.

Lindborg, L., J. E. Kyllonen, P. Beck, J. F. Bottollier-Depois, S. Gerdung, R. E. Grillmaier, and U. Schrewe (1999), The use of TEPC for reference dosimetry, *Radiat. Prot. Dosim.*, *86*, 285–8.

Lindstrom, C. D., J. D. Sullivan, B. K. Dichter, F. A. Hanser, D. Carssow, and G. E. Galica (2011), Characterization of Teledyne microdosimeters for space weather applications, *Proc. SPIE*, *8148*, 814,806, doi:10.1117/12.893814.

Mazur, J. E., W. R. Crain, M. D. Looper, D. J. Mabry, J. B. Blake, A. W. Case, M. J. Golightly, J. C. Kasper, and H. E. Spence (2011), New measurements of total ionizing dose in the lunar environment, *Space Weather 12*, S07002, doi:10.1029/2010SW000641.

Mertens, C. J., B. T. Kress, M. Wiltberger, S. R. Blattnig, T. S. Slaba, S. C. Solomon, and M. Engel (2010), Geomagnetic influence on aircraft radiation exposure during a solar energetic particle event in October 2003, *Space Weather 8*, S03006, doi:10.1029/2009SW000487.

Mertens, C. J., B. T. Kress, M. Wiltberger, W. K. Tobiska, B. Grajewski, and X. Xu (2012), Atmospheric ionizing radiation from galactic and solar cosmic rays, in *Ionizing Radiation/Book 2*, edited by M. Nenoi, InTech Publisher, Rijeka, Croatia.

Mertens, C. J., M. M. Meier, S. Brown, R. B. Norman, and X. Xu (2013), NAIRAS aircraft radiation model development, dose climatology, and initial validation, *Space Weather*, *11*, 1–33, doi:10.1002/swe.20100.

Mertens, C. J., et al. (2016), Cosmic radiation dose measurements from the RaD-X flight campaign, *Space Weather*, doi:10.1002/2016SW001407.

National Council on Radiation Protection and Measurements (NCRP) Commentary No. 12 (1995), Radiation exposure and high-altitude flight, National Council on Radiation Protection and Measurements, Bethesda, Md.

National Council on Radiation Protection and Measurements Report 132 (2000), Radiation protection guidance for activities in low-Earth orbit, National Council on Radiation Protection and Measurements, Bethesda, Md.

National Council on Radiation Protection and Measurements (NCRP) Report 153 (2006), Information needed to make radiation protection recommendations for space missions beyond low-Earth orbit, National Council on Radiation Protection and Measurements, Bethesda, Md.

National Council on Radiation Protection and Measurements Report 38 (1971), Protection against neutron radiation, National Council on Radiation Protection and Measurements, Bethesda, Md.

NIST (2016), National Institute of Standards and Technology, Washington, D. C. [Available at http://www.nist.gov/pml/data/xraycoef/, accessed February 2016.]

O'Brien, K., and W. Friedberg (1994), Atmospheric cosmic rays at aircraft altitudes, *Environ. Intl.*, *20*, 645–663.

Perez-Nunez, D., and L. A. Braby (2011), Replacement tissue-equivalent proportional counter for the international space station, *Radiat. Prot. Dosim.*, *143*, 394–397.

Reitz, G. (1993), Radiation environment in the stratosphere, *Radiat. Prot. Dosim.*, *48*, 5–20.

Schwadron, N. A., et al. (2012), Lunar radiation environment and space weathering from the Cosmic Ray Telescope for the Effects of Radiation (CRaTER), *J. Geophys. Res.*, *117*, E00H13, doi:10.1029/2011JE003978.

Standard Imaging (2008), Standard Imaging, Energy Dependence of Exradin A6 Spherical Ion Chamber. June 2008.

Spurny, F., and T. S. Dachev (2003), Long-term monitoring of the onboard aircraft exposure level with a Si-diode based spectrometer, *Adv. Space Res.*, *32*(1), 53–58.

Stassinopoulos, E. G., C. A. Stauffer, T. P. Dachev, G. J. Brucker, B. T. Tomov, and P. G. Dimitrov (2002), The Liulin-3M radiometer for measuring particle doses in space and on aircraft, NASA/TM-2002-210003.

Straume, T., J. C. McDonald, R. A. Pederson, D. J. Brenner, and R. L. Dobson (1991), Hiroshima-like neutrons from A-bomb replica: physical basis for their use in biological experiments, *Radiat. Res.*, *128*, 133–142.

Straume, T., L. A. Braby, T. B. Borak, T. Lusby, D. W. Warner, and D. Perez-Nunez (2015), Compact tissue-equivalent proportional counter for deep-space human missions, *Health Phys.*, *109*, 277–283.

Teledyne Microelectronic Technologies (2016), Teledyne Microelectronic Technologies. [Available at http://www.teledynemicro.com/documents/Datasheets/UDOS001_Micro_Dosimeter_Datasheet.pdf, accessed February 2016.]

Tobiska, W. K., et al. (2015), Advances in atmospheric radiation measurements and modeling needed to improve air safety, *Space Weather*, *13*, 202–210, doi:10.1002/2015SW001169.

Uchihori, Y., H. Kitamura, K. Fujitake, T. P. Dachev, B. T. Tomov, P. G. Dimitrov, and Y. Matviichuk (2002), Analysis of the calibration results obtained with Liulin-4 J spectrometer-dosimeter on protons and heavy ions, *Radiat. Meas.*, *35*, 127–134.

Wilson, J. W., J. E. Nealy, F. A. Cucinotta, J. Shinn, F. Hajnal, M. Reginatto, and P. Goldhagen (1995), Radiation safety aspects of commercial high-speed flight transportation, NASA Technical Paper 3524, NTIS, Springfield, Va.